Modeling of Wind Turbines Equipped with Doubly-Fed Induction Machines for Power System Stability Studies

I. Erlich, *Senior Member, IEEE*, and F. Shewarega

Abstract--**This paper deals with the modeling of the doubly-fed induction generator (DFIG) for stability studies. Using the space-phasor representation and the underlying quasi stationary model, suitable control algorithms for the simulation of the DFIG operating on an interconnected system is developed. The schemes include the pitch-angle/speed control and the decoupled control of the real and reactive power outputs. The model is then implemented on a large test network. Simulations have been carried out to study the control behavior of wind turbines to wind speed changes and the response to three phase grid faults. The results demonstrate the suitability of the models and the overall control architecture for stability studies and give insight into the scope of possible targeted control interventions. The short-circuit test in particular highlights the relationship between the control philosophy adopted and the possibility of the DFIG actively participating in supporting the network voltage.**

***Index Terms*--Wind power, control system, power system stability, doubly-fed induction machine.**

I. NOMENCLATURE

$\underline{i}$, $\underline{u}$	Complex current, voltage
$\underline{\psi}$,β	Complex flux-linkages, pitch angle
P, Q	Real, reactive power
l, x	Inductance, reactance
r, z	Resistance, impedance
ω, s	Angular speed, slip
t, T	Torque, time constant
v_w	Wind speed
Superscripts/subscripts	
‘	Transient inductance/variable
S, R	Stator, rotor
d, q	Direct, quadrature axis component
h, σ	Main field, leakage
K, 0	Arbitrary, synchronous reference frame
m, el	Mechanical, electrical

II. INTRODUCTION

THE past decade has seen the emergence of wind as the world’s most dynamically growing energy source. This trend has continued unabated into the current decade. In 2003 and 2004, the installed worldwide wind energy capacity grew by 26% and 20%, respectively. Whilst by the end of the year 2002 in all 31,117 MW were installed, this figure went up to 47,305 MW at the end of 2004, and the 50,000 MW mark was surpassed by mid-2005. According to the World Wind Energy Association (WWEA) forecast, an aggregate installed wind energy capacity of 100,000 MW is expected to be reached in the year 2008. Wind power has, in the process of this rapid expansion, moved from being an unconventional technology to the mainstream of power generation.

This paper deals with the modeling of wind generation plants equipped with doubly-fed induction generators (DFIG) for stability studies. Various papers have been published dwelling on modeling of the DFIG in the past [1]-[13].The common feature in all the papers has been the field oriented control (FOC), which enables the decoupled control of active and reactive power outputs. However most of the papers restrict the analysis to individual units and thus the corresponding simulation techniques are not offhand adaptable to large power systems consisting of hundreds or thousand of wind turbines as well as conventional synchronous generators. Stability study is becoming particularly important given the fact that utilities have to ensure the same stability margin even in cases where wind power constitutes a significant component of the total power generation.

The dynamic DFIG model can, as a first approximation, be considered comparable to that of conventional synchronous generators. Just like in the case of conventional generators, these models must on the one hand be simple enough to allow simulation of large number of wind turbines and should on the other hand account for all phenomena relevant to system performance. Moreover, simulations have to be carried out often in the planning stage where no reliable information about the wind turbines and the associated control system are available. In such cases “standard models” lend themselves as a possible alternative.

This paper is aimed at providing an exhaustive overview of the current state-of-the-art in modeling the DFIG for large-scale system studies. Based on this survey the control system of the DFIG vis-à-vis its capability to mitigate the impact of a contingency situation on the power system will be outlined and corroborated using an example.

The paper is structured as follows. Following this introduction the quasi-stationary model of the DFIG will be

I. Erlich is with the University Duisburg-Essen, 47057 Duisburg, Germany (e-mail: erlich@uni-duisburg.de);
F. Shewarega is with the University Duisburg-Essen, 47057 Duisburg, Germany, (e-mail: shewarega@uni-duisburg.de).

derived starting from the detailed equations. Then, the control structure will be discussed, which includes the speed and pitch-angle control as well as the fast, decoupled electrical control of P and Q. To validate and demonstrate the applicability of the models developed, some simulation examples are presented at the end.

III. MODEL OF THE DFIG

A. Detailed DFIG model

The DFIG is the most commonly used device for wind power generation. As is generally known, the rotor terminals are fed with a symmetrical three-phase voltage of variable frequency and amplitude. This voltage is supplied by a voltage source converter usually equipped with IGBT based power electronic circuitry. The basic structure is shown in Fig. 1.

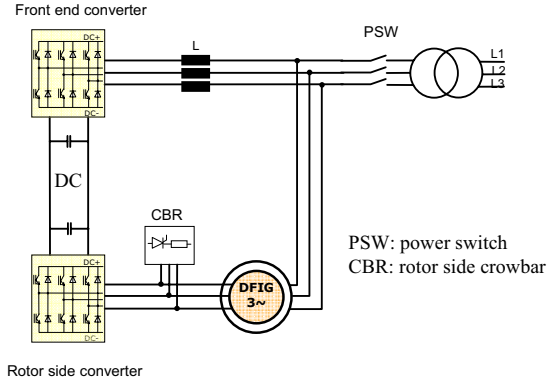

Figure 1. Structure of the DFIG based wind system

The variable rotor voltage permits the adjustment of the rotor speed to match the optimum operating point at any practical wind speed. The necessary rotor power for adjusting the speed depends on the desired speed range (Δω), which is given by the range between cut-in and maximum wind speeds. The converter enables the machine to operate in all four quadrants in the complex PQ-plane, which implies that the machine is capable of delivering reactive power to the grid (as opposed to the ordinary induction machine). On top of this, the reactive power exchange with the grid can be controlled independently from the real power.

Protection against overcurrents and undesirably high DC voltage is provided by the crowbar (CBR) placed on the rotor side. When the current limit is exceeded the CBR thyristor switch is fired and the rotor terminals are short-circuited through the CBR resistance. During this period the control action of the converter is trimmed to shut down and allow the DFIM to operate as a conventional slip-ring induction machine. The DFIM during this phase becomes a reactive power consumer. Because the initialization of the CBR is based on rotor current instantaneous values and DC voltage, the stability models developed in the next chapter will not be able to reproduce the correct timing of CBR firing procedure. However, the CBR switching sequence can be based on a preset time schedule or on a simplified initialization criterion.

The theoretical background for modeling induction machines are widely developed and are exhaustively dealt with in numerous papers and textbooks. In this paper, the space phasor representation using complex vectors (underlined variables) containing orthogonal direct (d) and quadrature (q) axis components is adopted. Phasors can be represented with respect to different rotating reference frames and the reference axis may be fixed at any point in the complex plane. The choice of the reference system has a direct bearing on the realization of the desired decoupled control of P and Q. The reference frame for each of the complex variables will be signified using a superscript $\angle$ and possibly followed by u or Ψ to denote that the d-axis corresponds with the location of the phasors $\underline{u}$ and $\underline{\Psi}$ respectively

Equations (1) - (5) represent the complete set of mathematical relationships that describe the dynamic behavior of the machine. The per-unit (p.u.) system is adopted as a unit of measurement for all quantities and the sign convention is chosen in such a way that consumed active and inductive reactive powers are positive. (Note also that ω_0 is equal to 1.0 in p.u.)

Voltage equations:

$$\underline{u}_S^{\angle} = r_S \cdot \underline{i}_S^{\angle} + \frac{d\underline{\psi}_S^{\angle}}{dt} + j \cdot \omega_K \cdot \underline{\psi}_S^{\angle} \tag{1}$$

$$\underline{u}_R^{\angle} = r_R \cdot \underline{i}_R^{\angle} + \frac{d\underline{\psi}_R^{\angle}}{dt} + j \cdot (\omega_K - \omega_R) \cdot \underline{\psi}_R^{\angle} \tag{2}$$

ω_K is an arbitrary speed corresponding to the speed of the rotating reference frame.

Flux linkages:

$$\underline{\psi}_S^{\angle} = l_S \cdot \underline{i}_S^{\angle} + l_h \cdot \underline{i}_R^{\angle} \tag{3}$$

$$\underline{\psi}_R^{\angle} = l_h \cdot \underline{i}_S^{\angle} + l_R \cdot \underline{i}_R^{\angle} \tag{4}$$

where $l_S = l_h + l_{\sigma S}$ and $l_R = l_h + l_{\sigma R}$

Equation of motion:

$$\frac{d\omega_R}{dt} = \frac{1}{T_m}\left(\psi_{Sd}^{\angle} i_{Sq}^{\angle} - \psi_{Sq}^{\angle} i_{Sd}^{\angle} + t_m\right) \tag{5}$$

The nomenclature of all symbols used in the above equations and the equations to follow is given at the beginning of the paper.

Equations (1) and (2) resolved into real and imaginary parts together with (5) constitute the 5th order model of the doubly-fed induction machine. The stator terminal voltage $\underline{u}_S^{\angle}$ forms the link to the rest of the network. The use of the 5th order model for the machine is premised on the assumption that differential equations are used for the whole network and computations are carried out using instantaneous values, which, for obvious reasons, is not suitable for large scale stability simulation.

B. Reduced order dynamic model

The reduced order or the so-called quasi stationary model can then be obtained by neglecting the derivative term in (1),

i.e. $\frac{d\underline{\psi}_S^{\angle\omega_0}}{dt} \approx 0$. This approximation is warranted in the synchronously rotating reference frame only [14]. Accordingly, from this point onwards the synchronously rotating reference frame will be adopted but the superscript $\angle\omega_0$ will be abandoned for simplicity of notation. It then follows from (1) for the stator flux linkages:

$$\underline{\psi}_S = \frac{\underline{u}_S - r_S \underline{i}_S}{j\omega_0} \tag{6}$$

Similarly, another expression for the stator flux linkages can be obtained by eliminating the rotor current in (3) using (4). Thus,

$$\underline{\psi}_S = l_S \underline{i}_S + \left(\underline{\psi}_R - l_h \underline{i}_S\right)\frac{l_h}{l_R} \tag{7}$$

From Eq. (6) and (7) we have:

$$\underline{u}_S - r_s \underline{i}_S = j\omega_0 \left[l_S \underline{i}_S + \left(\underline{\psi}_R - l_h \underline{i}_S\right)\frac{l_h}{l_R} \right], \tag{8a}$$

which, after rearrangement, results in:

$$\underline{u}_S = \underline{z}' \, \underline{i}_S + \underline{u}' \tag{8b}$$

where

$$\underline{z}' = \left(r_S + j\omega_0 l'\right) \tag{9}$$

is defined as the internal transient impedance and

$$\underline{u}' = j\omega_0 k_R \underline{\psi}_R \tag{10}$$

is the driving transient Thévenin voltage source, with

$$l' = l_s - \frac{l_h^2}{l_R} \quad \text{and} \quad k_R = \frac{l_h}{l_R}$$

The voltage equation (8b) can be illustrated using the equivalent circuit given in Fig. 2.

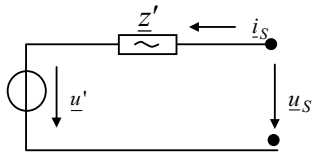

Figure 2. Quasi-stationary equivalent circuit of the DFIM

The internal voltage in Fig. 2 ($\underline{u}'$) is a function of the d- and q-components of the rotor flux, which together with the rotor speed are state variables of the reduced order model. The state-space differential equations themselves can be obtained from (2) after eliminating the rotor current using (4). The resulting relationship separated into d- and q-components is:

$$\frac{d\psi_{Rd}}{dt} = -\frac{r_R}{l_R}\psi_{Rd} + \left(\omega_R - \omega_0\right)\psi_{Rq} + k_R r_R i_{Sd} + u_{Rd} \tag{11}$$

$$\frac{d\psi_{Rq}}{dt} = \left(\omega_R - \omega_0\right)\psi_{Rd} - \frac{r_R}{l_R}\psi_{Rq} + k_R r_R i_{Sq} + u_{Rq} \tag{12}$$

To complete the quasi stationary model, the equation of motion (5) needs to be modified to take account of the fact that the stator flux is now no more a state variable. This is achieved by eliminating the stator flux first using (3) and then the rotor current using (4), which results in:

$$\frac{d\omega_R}{dt} = \frac{1}{T_m}\left[k_R\left(\psi_{Rd} i_{Sq} - \psi_{Rq} i_{Sd}\right) + t_m\right] \tag{13}$$

Equations (11)-(13) constitute the quasi-stationary (3rd order) model of the induction machine. The determination of the rotor flux linkages $\underline{\psi}_R$ and thus the stator current $\underline{i}_S$ requires the numerical integration of (11) and (12) and the solution of the load flow equations of the network into which the machine equivalent circuit (Fig. 2) is incorporated. The equation of motion (13) has to be solved simultaneously with (11) and (12) to obtain the rotor speed.

C. Stationary model

The equations valid in the steady-state are obtained by neglecting the transformer voltages not only in (1) but also in (2). It follows from (2) together with (4) that:

$$\frac{\underline{u}_R}{s} = \frac{r_R}{s}\underline{i}_R + j\omega_0\left(l_h \underline{i}_S + l_R \underline{i}_R\right) = \frac{r_R}{s}\underline{i}_R + jx_h \underline{i}_S + jx_R \underline{i}_R \tag{14}$$

where the slip

$$s = \left(\omega_0 - \omega_R\right)/\,\omega_0 \tag{15}$$

is introduced. Eq. (8a) represents the steady-state equation for the stator winding. Eliminating the rotor flux in (8a) using (4), we have:

$$\underline{u}_S = r_S \underline{i}_S + j\omega_0 \cdot \left(l_S \underline{i}_S + l_h \underline{i}_R\right) = r_S \underline{i}_S + jx_S \underline{i}_S + jx_h \underline{i}_R \tag{16}$$

The voltage equations (14) and (16) translate into the familiar equivalent circuit of an induction machine, which is given in Fig. 3.

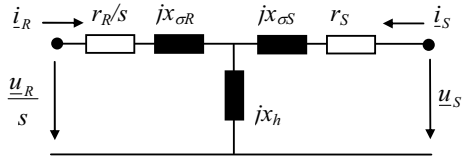

Figure 3. Equivalent circuit of the doubly-fed induction machine in steady-state.

It should be noted that the steady-state model is not suitable for dynamic studies. However, it is essential for a better understanding of the DFIM characteristics and its operating principles.

IV. MODELLING OF THE CONTROL SYSTEM

The control system of the doubly-fed induction machine encompasses the speed/pitch-angle control and the control systems associated with the grid side as well as the rotor side converters.

A. Speed/pitch- angle control and model of the wind power conversion

The mechanical power extracted from the wind can be calculated as:

$$p_T = \frac{1}{2}\rho \, A_{rot} C_p(\lambda, \beta) v_w^3 \tag{17}$$

where

- ρ air density
- A_{rot} cross-section through which the air mass is streaming
- Cp power coefficient
- v_W wind speed

Wind turbine manufacturers give the specific value of Cp for a turbine usually as a function of the pitch-angle β and tip-speed

ratio λ. The tip-speed ratio is defined as:

$$\lambda = \omega_T R / v_w \tag{18}$$

R is the radius and ω_T is the speed of the turbine. There is a fixed relationship between ω_T and ω_R given by the gear transmission ratio.

Wind turbines provide two degrees of freedom for control, namely turbine speed (which is proportional to the rotor speed) and the blade pitch-angle. Depending on the actual wind speed, one can distinguish between partial and full load modes. At partial loads the pitch angle is adjusted for capturing the maximum wind power [13]. The corresponding pitch angle is almost constant although the rotor speed is required to change to adapt to the actual wind speed. The rotor speed can vary between a certain minimum and the maximum allowable values. At very low wind speeds, the turbine speed must be fixed at the lowest minimum limit. If the maximum speed is already reached at a particular partial load, it is required to be held constant at that value for all higher wind speeds. The upper part of Fig. 4 shows a possible control structure for keeping the rotor speed within the desired range. The output of this controller serves as the set point for the rotor side converter control.

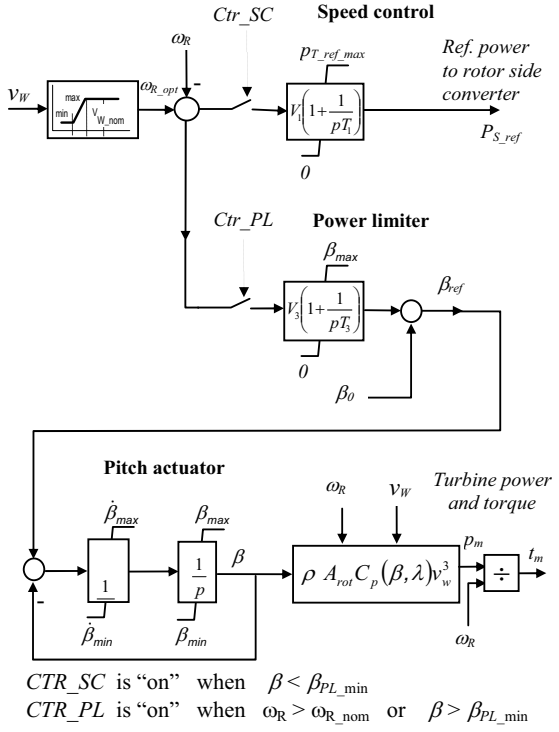

Figure 4. Wind converter model and control

At wind speeds of about 12 m/s the maximum turbine power is reached. Beyond this limit the blades have to be turned towards higher pitch angles for limiting the torque to the maximum permissible value. This can be achieved again by a speed control that keeps turbine speed at its nominal value. Both partial and full load turbine controls can be modeled by the schema shown in Fig. 4.

The optimal rotor speed depending on the wind speed is described by a characteristic lookup table shown in the upper left corner (Fig. 4). When the nominal wind speed is reached (approximately at 12 m/s) the lower speed controller is activated to pitch the blades and thus to reduce the power generated. The angle β_0 represents the set point in partial load mode. The output β_{ref} is provided to the blade actuator which is represented by a first order delay. The corresponding model is split into two parts to take account of limitations on both the absolute value of the pitch-angle and its gradient [13]. The calculation of the turbine power p_m and torque t_m is needed only for the evaluation of Eq. (13).

Wind turbine control may differ from manufacturer to manufacturer depending on the control philosophy adopted and the way it is implemented. In [13] a detailed description about the main issues related to wind turbine control is provided. Furthermore, a control structure is presented that does not need wind speed measurements. (The accuracy of wind speed measurements is limited anyway.) For quantitative simulation studies the use of specific information provided by the manufactures is always recommended.

B. Control and modeling of the rotor side converter

The rotor side converter is used to control the real and reactive power outputs of the machine. The extraction of maximum energy from the wind necessitates the adjustment of the rotor speed to correspond to the changing wind speed. Therefore, the reference power provided to the converter control is derived from the wind speed based on a characteristic diagram shown in Fig. 4.

Independent control of P and Q can be achieved through rotor current control as will be shown a little later in the paper. As can be seen in Eq. (5) the electrical torque keeping balance with the mechanical turbine torque is calculated using the equation:

$$t_{el} = \psi_{Sd}^{\angle} i_{Sq}^{\angle} - \psi_{Sq}^{\angle} i_{Sd}^{\angle} \tag{19}$$

Assuming an orthogonal coordinate system where the real axis always corresponds with the direction of the stator flux, i.e.,

$$\psi_{Sd}^{\angle \psi_S} = \left| \underline{\psi}_S \right| \tag{20}$$

$$\psi_{Sq}^{\angle \psi_S} = 0 \tag{21}$$

we have

$$t_{el} = \left| \underline{\psi}_S \right| i_{Sq}^{\angle \psi_S} \tag{22}$$

One can easily deduce that the control of electrical torque can be brought about through the control of the q-axis component of the stator current.

Locating the d-axis along the stator flux is a common practice in electrical drives. However, power engineers are more familiar with active and reactive currents. To take account of this preference, the stator voltage can be oriented along the d-axis. It then follows from Eq. (6) for the stator flux and voltage:

$$\underline{u}_S = r_S \underline{i}_S + j\omega_0 \underline{\psi}_S \tag{23}$$

Introducing a slightly modified version of the stator voltage

$$\underline{u}_{SR} = \underline{u}_S - r_S \underline{i}_S = j\omega_0 \underline{\psi}_S \tag{24}$$

we observe that the stator flux linkage lags by π/2 behind the stator voltage $\underline{u}_{SR}$. Thus $i_{Sq}^{\angle\psi_S}$ becomes $i_{Sd}^{\angle u_{SR}}$ if $\underline{u}_{SR}$ is chosen as the d-axis. As a result, the torque equation (22) now becomes:

$$t_{el} = \left|\underline{\psi}_S\right| i_{Sd}^{\angle u_{SR}} \tag{25}$$

$i_{Sd}^{\angle u_{SR}}$ corresponds with the well known active current and the imaginary component $i_{Sq}^{\angle u_{SR}}$ with the negative of the reactive current.

Further simplification is possible by considering the fact that the voltage drop over the stator resistance is always small for the type of large machines employed in wind turbines, viz.

$$\underline{u}_{SR} \approx \underline{u}_S \tag{26}$$

Accordingly, $\underline{u}_S$ (instead of $\underline{u}_{SR}$) will be used as the reference in the subsequent sections. (For a more stringent accuracy requirement, all that is needed is the replacement of $\underline{u}_S$ by $\underline{u}_{SR}$ in the corresponding equations.) Fig. 5 shows the phasor diagram and the relationships in the stator voltage oriented reference frame.

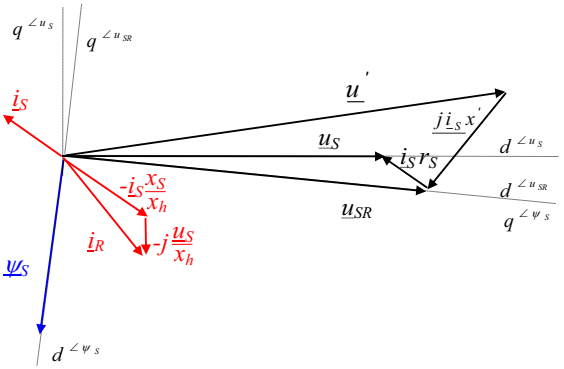

Figure 5. Phasor diagram and definition of different reference frames

Control of the DFIG takes place essentially from the rotor side. To calculate the reference values for rotor currents, the steady state relationship between rotor and stator currents is required. From Eq. (1) and (3) follows (after neglecting the derivative term and setting r_S=0):

$$\underline{i}_R^{\angle} = -\frac{x_S}{x_h}\underline{i}_S^{\angle} - j\frac{\underline{u}_S^{\angle}}{x_h} \tag{27}$$

In stator voltage oriented coordinates

$$i_{Rd}^{\angle u_S} = -\frac{x_S}{x_h} i_{Sd}^{\angle u_S} \tag{28}$$

$$i_{Rq}^{\angle u_S} = -\frac{x_S}{x_h} i_{Sq}^{\angle u_S} - \frac{\left|\underline{u}_S\right|}{x_h} \tag{29}$$

Assuming that the reference values for active and reactive stator power outputs are known, the corresponding rotor reference currents can be calculated as:

$$i_{Rd\_ref}^{\angle u_S} = -\frac{p_{S\_ref}}{\left|\underline{u}_S\right|}\frac{x_S}{x_h} \tag{30}$$

$$i_{Rq\_ref}^{\angle u_S} = \frac{q_{S\_ref}}{\left|\underline{u}_S\right|}\frac{x_S}{x_h} - \frac{\left|\underline{u}_S\right|}{x_h} \tag{31}$$

Practical requirements dictate that a delay term is introduced before passing p_{S_ref} and q_{S_ref} on to the current controller. The term $\frac{\left|\underline{u}_S\right|}{x_h}$ represents the magnetization current that additionally has to be provided from the rotor side. Fig. 6 shows the control and simulation structure derived from Eq. (30) and (31).

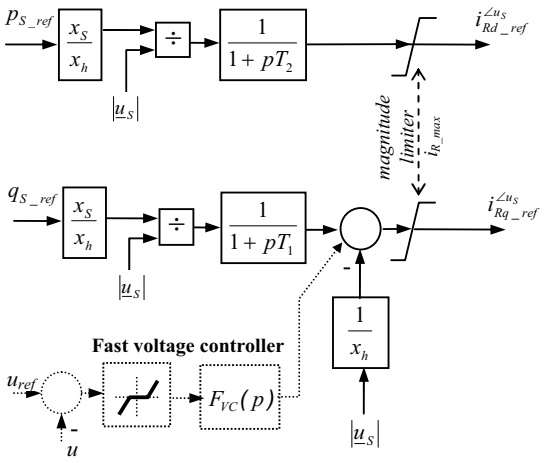

Figure 6. Structure for generating rotor current reference values

The magnitude limiter shown in Fig 6 considers the maximum permissible rotor current. It is not specifically related to d- or q-components but limits the resultant, i.e. the current magnitude. In case the current limit is exceeded, either P or Q may be singled out for reduction, depending on which option is more expedient at the given condition. One of the common methods is to reduce both components equally so that their phase angle remains unchanged.

With increasing penetration and diffusion of wind turbines in the power system, the voltage control capability of the DFIG has become an important issue. The concern of the utilities is related to the fact that currently the DFIG provides restricted voltage support during short circuits and other low voltage periods. Generally, wind generators are able to control the voltage as long as the current is within limits and of course the machines remain connected to the grid during the fault (fault ride-through capability). However, the maximum allowable current is normally just slightly above the nominal value. Besides, the power converters do not tolerate considerable overloads. Generally speaking there is a possibility to increase the reactive current temporarily to compensate for the active power reduction arising from the fact that the real power is controlled towards a lower value by the rotor side converter during this time span. However, to avoid undesirable rotor speed increase the active power must be restored within a few seconds.

Fig. 6 has been augmented by a fast-acting voltage controller. The chosen gain and time constant depend on the stability requirements of the system that has always to be guaranteed. Sometimes it is reasonable to include a dead band into the voltage control loop to avoid unnecessary control actions. With continuously acting control on the other hand voltage fluctuation caused by the wind can be smoothed. At

this point it should be mentioned that the voltage to be controlled can differ from the terminal voltage. So, with some restrictions, the wind turbines are able to control voltages at network nodes at some distance from their location.

The next question concerns the control loop of the rotor current and how the corresponding rotor voltage is calculated. The rotor voltage is provided by the rotor side converter based on the so-called vector control. This part works so fast that any time delay in the dynamic model of the converter would be superfluous.

From (14), (16) follows (with $r_S = 0$)

$$\underline{u}_R = r_R \cdot \underline{i}_R + js \cdot \left(x_h \cdot \frac{\underline{u}_S - jx_h \cdot \underline{i}_R}{jx_S} + x_R \cdot \underline{i}_R \right) \tag{32}$$

Considering a coordinate system where the d axis is located along $\underline{u}_S$, we have

$$u_{Rd}^{\angle u_S} = r_R i_{Rd}^{\angle u_S} + s \left(\frac{x_h}{x_S} |\underline{u}_S| - i_{Rq}^{\angle u_S} \; \sigma \; x_R \right) \cdot \tag{33}$$

$$u_{Rq}^{\angle u_S} = r_R i_{Rq}^{\angle u_S} + s \; i_{Rd}^{\angle u_S} \; \sigma \; x_R \tag{34}$$

where leakage coefficient $\sigma = \left(1 - x_h^2 / x_R x_S\right)$ is introduced.

The voltage drops over the rotor resistance in (33) (34) can be interpreted as auxiliary signals which are outputs of the intended rotor current controller [2]. Assuming PI controllers, the control transfer function is as follows:

$$u'^{\angle u_S}_{Rd} = r_R i_{Rd}^{\angle u_S} = K_I \left(1 + \frac{1}{pT_I} \right) \cdot \left(i_{Rd\_ref}^{\angle u_S} - i_{Rd}^{\angle u_S} \right) \tag{35}$$

$$u'^{\angle u_S}_{Rq} = r_R i_{Rq}^{\angle u_S} = K_I \left(1 + \frac{1}{pT_I} \right) \cdot \left(i_{Rq\_ref}^{\angle u_S} - i_{Rq}^{\angle u_S} \right) \tag{36}$$

The corresponding block diagram of the rotor current controller is shown in Fig. 7.

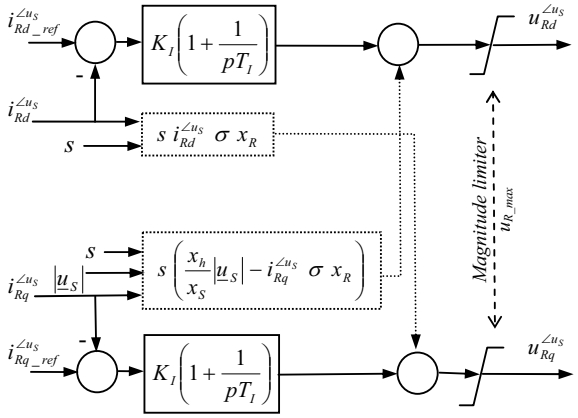

Figure 7. Rotor current control

To be able to pass the outputs $u_{Rd}^{\angle u_S}$ and $u_{Rq}^{\angle u_S}$ in a practical situation as reference values to the rotor side converter control, the signals have to be transformed into the rotor reference frame, which necessitates knowledge of the rotor (position) angle. However, algorithms for power system dynamic simulations usually define a common, synchronously with ω_0 rotating reference frame just as is the case in this paper. Because of their symmetrical layout induction machines can be described in this synchronous reference frame as well, as indicated in chapter III. Therefore, in a simulation algorithm the outputs of the current controller have to be transformed to this common reference frame merely in accordance with (37)

$$\underline{u}_R = \underline{u}_R^{\angle u_S} \; e^{j\varphi_{us}} \tag{37}$$

where φ_{us} represents the stator voltage angle. Then, $\underline{u}_R$ can be passed on to the corresponding state equation (11), (12) which are described in the common synchronous reference frame. (Recall that phasors are not labeled when referred to the common synchronous reference frame.) It should also be noted that the same transformation (but in the inverse direction) is needed for calculation of $i_R^{\angle u_S}$ from $\underline{i}_R$

Analogous to the limitation of the rotor reference current shown in Fig. 6, the magnitude of the rotor voltage must be limited as well. However, when the maximum available rotor voltage is reached a signal must be sent to the PI controller to stop further integration.

The current controller also contains cross-coupling terms (dotted boxes) as shown in Fig. 7. As opposed to the conventional wisdom, these signals are usually not quite insignificant. The common practice of neglecting them is justified all the same on account of the fact that the PI current controllers with common gain and time constant are able to compensate for the missing cross-coupling signals without considerable control error. Fig. 8 shows an example to demonstrate the effect of the cross-coupling terms.

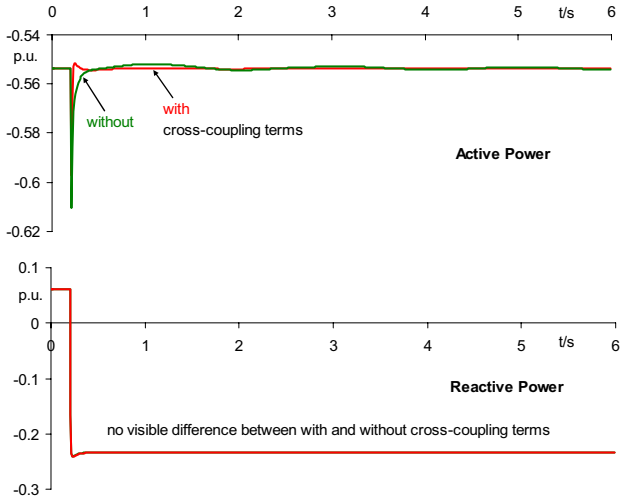

Figure 8. Step response to $i_{Rq\_ref}^{\angle u_S} = -0.3\ p.u.$ with and without cross-coupling terms; (slip(0) = -0.108532)

C. Control and modeling of the grid side converter

The grid and rotor side converters are linked through a DC circuit comprising of capacitances. If the DC voltage is assumed not to exceed certain limits, which otherwise would impose limitations on the capability of the controllers or initiate action by the protection system, an explicit representation of the DC circuit can be omitted for stability kind of power system simulations.

The control of the grid side converter is similar to that of the rotor side. However, in the active power channel the DC voltage is controlled. This is achieved when the active power passing through both converters (viz. the grid side and the rotor side) is in equilibrium. Therefore, the grid side converter will try to inject the same active power into the grid as that provided to the DFIG through the rotor side converter. Following the assumption that DC voltage fluctuations are not considered, the active power is injected into the grid without any time lag. After neglecting converter losses, we have for the corresponding power:

$$p_{CG} = p_R = u_{Rd}^{\angle} i_{Rd}^{\angle} + u_{Rq}^{\angle} i_{Rq}^{\angle} \tag{38}$$

In many publications the following approximation is used

$$p_{CG} = p_R \approx -sp_S \tag{39}$$

which, however, is only valid when the grid frequency remains constant at ω_0. Besides, the resistive losses are also neglected. In power system stability studies constant grid frequency cannot be guaranteed. Therefore, it is more accurate to use. (38) rather than (39).

The reactive power control channel of the grid side converter provides the capability to generate reactive power. Basically it works like a static compensator (STATCOM). However, in normal operation it is more purposeful to generate reactive power using the rotor side converter. The current transmitted from the rotor to the stator circuits is amplified on account of the characteristic value of the turns-ratio of the DFIG. Thus, the same reactive current passing through the rotor side converter is capable of producing higher reactive power compared to the current through the grid side converter. As a result, in normal operation, the reactive power reference value of the grid side converter is usually set to zero and the total reactive current required is supplied by the rotor side converter. However, during a disturbance or when stator circuit is disconnected for a short period of time [15], the grid side converter can be activated to provide reactive power support. Fig. 9 shows a simple model of the grid side converter applicable for stability studies.

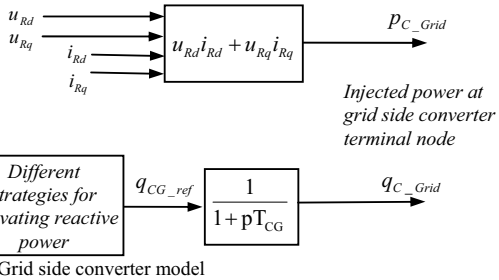

Figure 9. Grid side converter model

V. Simulation Examples

The following examples are primarily intended to validate the model introduced in this paper. Moreover, the examples should also highlight the fundamental differences between the dynamic performance of the DFIG and the conventional synchronous generators. As a test system, a 16-machine network [16] was used. To simulate the impact of wind farms on the dynamics of the overall system, one of the conventional power plants was replaced by a large wind farm, consisting of 528 units with a total installed capacity of 1650 MW. The constituent wind units are then represented by an equivalent single machine. The wind farm is connected to the 380-kV-line through a 150-kV cable, which in turn is supplied from 33-kV cables that interconnect the units within a farm and of course the associated transformers.

The first example in Fig. 10 shows the response of the DFIG to wind speed ramps. The wind speed is increased linearly from 10 m/s to approximately 13.5 m/s within a time span of 2.4 s. The wind speed then drops back to the initial value after a further 20 s. Because the wind speed exceeds the partial load limit of 12 m/s, the control mode changes from partial load to full load limiting the generated power. When the wind speed drops, the pitch control reduces the pitch-angle. However, this process is relatively slow and cannot keep pace with the drop in wind speed assumed for this simulation. As a result, the rotor-speed falls below the nominal value. After the speed controller takes over the control, the reference power is reduced for a short duration (sharp drop in Fig. 10) which results in the recovery of the speed and the stabilization of the system at the new partial load operating point, which is identical with that at the beginning.

The second example in Fig. 11 shows the response of the DFIG to a distance 3-phase short circuit in the 380-kV line. To provide voltage support during low voltage periods, the DFIG has been extended by a fast, continuously acting PI voltage controller in accordance with Fig. 6. The maximum short term rotor current is limited to 1.2 p.u. The results demonstrate the possibility of voltage control and the positive impact on the voltage profile that this action would have. The wind farm with such a voltage control capability is obviously strong enough to even out the electromechanical oscillations caused by conventional synchronous generators. In this example the simulation has been carried out including speed and pitch angle controllers. However, tests have shown that their effect on the DFIG response is small and the assumption of a constant reference power p_{S_ref} would be, in this case, justified.

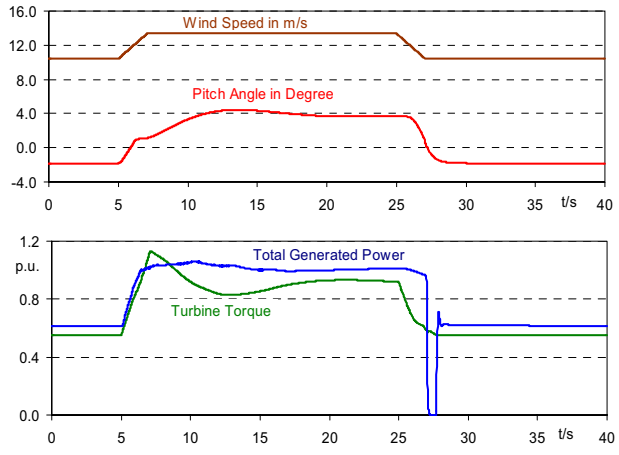

Figure 10. Response of DFIG to simulated wind speed ramps

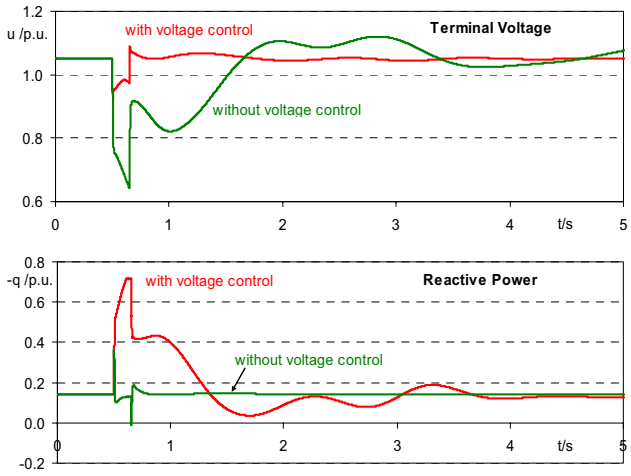

Figure 11. Response of DFIG to a 3-phase fault with and without voltage control

VI. CONCLUSION

The modelling of the DFIG in power system stability studies is the focus of this paper. The quasi stationary model based on space-phasor representation was expanded to include models for the speed/pitch angle control and those associated with the grid and rotor side converters. The control algorithms were derived with the need for wind plants to actively support the network voltage profile during a contingency situation in mind, in addition to the routinely employed decoupled control of the real and reactive power outputs of the machine.

To validate the models, some simulations were carried out on a representative 16 machine network. The first of the test examples involved a wind speed ramp triggered the control to change between speed and power limitation control. The next example deals with a three-phase short circuit in the grid. The results demonstrate the adequacy of the model and the underlying control architecture. The short-circuit test in particular underlines the capability of the DFIG- with a suitable control structure- to actively participate in supporting the network voltage, in addition to enhancing its own fault ride-through capability.

VII. REFERENCES

[1] M.A. Pöller, "Doubly-Fed Induction Machine Models for Stability Assessment of Wind Farms", in *Proc. IEEE PowerTech, Bologna*, Italy, June, 2003, BPT0-345

[2] A. Mullane, M. O´Malley, "The Inertial Response of Induction-Machine-Based Wind Turbines", *IEEE Trans. Power Systems*, vol. 20, pp. 1496-1503, Aug. 2005.

[3] A. D. Hansen, F. Iov, P. Sorensen, F. Blaabjerg, „Overall control strategy of variable speed doubly-fed induction generator wind turbine", Nordic wind Power Conference, 1-2 March, 2004, Chalmers University of Technology

[4] T. Sun, Z. Chen, F. Blaabjerg, „ Transient Analysis of Grid-Connected Wind Turbines with DFIG After an External short-Circuit Fault", Nordic wind Power Conference. 1-2 March, 2004, Chalmers University of Technology

[5] F. M. Hughes, O. Anaya-Lara, N. Jenkins, G. Strbac, "Control of DFIG-Based Wind Generation for Power Network Support", ," *IEEE Trans. Power Systems*, vol. 20, pp. 1958-1966, Nov. 2005.

[6] P. Ledesma, J. Usaola, "Effect of Neglecting Stator Transients in Doubly Fed Induction Generator Models", *IEEE Trans. on Energy Conversion*, vol. 19, pp. 459-461, Jun. 2004.

[7] P. Ledesma, J. Usaola, "Doubly Fed Induction Generator Model for Transient Stability Analysis", *IEEE Trans. on Energy Conversion*, vol. 20, pp. 388-397, Jun. 2005.

[8] L. Holdsworth, X. G. Wu, J. B. Ekanayake, N. Jenkins, "Direct solution method for initializing doubly-fed induction wind turbines in power system dynamic models", *IEE Proc.-Gener. Transm. Distrib.* vol. 150, pp. 334-342, May. 2003

[9] J. B. Ekanayake, L. Holdsworth, X.G. Wu, N. Jenkins, "Dynamic Modeling of Doubly Fed Induction Generator Wind Turbines", *IEEE Trans. on Power Systems* vol. 18, pp. 803-809, May. 2003.

[10] Y. Lei, A. Mullane, G. Lightbody, R. Yacamini, " Modeling of the Wind Turbine With a Doubly Fed Induction Generator for Grid Integration Studies", *IEEE Trans. on Energy Conversion*, vol. 21, pp. 256-264, March. 2006.

[11] T. Sun, Z. Chen, F. Blaabjerg, „Voltage Recovery of Grid-Connected Wind Turbines with DFIG After a Short-Circuit Fault", *35th Annual IEEE Power Electronics Conference*, Aachen, Germany, 2004, pp. 1991-1997.

[12] P. Cartwright, L. Holdsworth, J.B. Ekanayake, N. Jenkins, "Co-ordinated voltage control strategy for a doubly-fed induction generator (DFIG)-based wind farm" ", *IEE Proc.-Gener. Transm. Distrib.* vol. 151, pp. 495-502, July. 2004

[13] A. D. Hansen, C. Jauch, P. Sorensen, F. Iov, F. Blaabjerg, „Dynamic wind turbine models in power system simulation tool DIgSILENT", Risø National Laboratory, Roskilde, December 2003, ISBN 87-550-3199-4, Available: http://www.risoe.dk/rispubl/VEA/ris-r-1400.htm

[14] I. Erlich, H. Pundt, S. Djumena, " A new Synchronous Generator Model for Power System Stability analysis" *12th Power System Computation Conference*, Dresden, August 19-23, 1996, pp. 1062-1068

[15] I. Erlich, W. Winter, A. Dittrich „Advanced Grid Requirements for the Integration of Wind Turbines into the German Transmission System" IEEE-PES General Meeting Montreal 2006, panel paper 06GM0837

[16] S.P. Teeuwsen, I. Erlich, M.A. El-Sharkawi, "Neural Network based Classification Method for Small-Signal Stability Assessment", in *Proc. IEEE PowerTech, Bologna*, Italy, June, 2003, BPT03-151

VIII. BIOGRAPHIES

Istvan Erlich (1953) received his Dipl.-Ing. degree in electrical engineering from the University of Dresden/Germany in 1976. After his studies, he worked in Hungary in the field of electrical distribution networks. From 1979 to 1991, he joined the Department of Electrical Power Systems of the University of Dresden again, where he received his PhD degree in 1983. In the period of 1991 to 1998, he worked with the consulting company EAB in Berlin and the Fraunhofer Institute IITB Dresden respectively. During this time, he also had a teaching assignment at the University of Dresden. Since 1998, he is Professor and head of the Institute of Electrical Power Systems at the University of Duisburg-Essen/Germany. His major scientific interest is focused on power system stability and control, modelling and simulation of power system dynamics including intelligent system applications. He is a member of VDE and senior member of IEEE.

Fekadu Shewarega (1956) received his Dipl.-Ing. degree in electrical engineering from the Technical University of Dresden, Germany in 1985. From 1985 to 1988 he pursued his postgraduate studies at the same university in the area of the simulation of power system dynamics and obtained his PhD degree in 1988. After graduation, he joined the Addis Ababa University, Ethiopia as the member of the academic staff where he served in various capacities. Currently he is a member of the research staff at the University Duisburg – Essen. His research interests are focused on power system analysis and renewable energy technologies.